Patient-Informed Organ Dose Estimation in Clinical CT: Implementation and Effective Dose Assessment in 1048 Clinical Patients

Wanyi Fu, MS[1,2,3], Francesco Ria, PhD[3,4], William Paul Segars, PhD[1,3,5,6], Kingshuk Roy Choudhury, PhD[3], Joshua M. Wilson, PhD[4,5], Anuj J. Kapadia, PhD[1,3,5,7], Ehsan Samei, PhD[1,2,3,4,5,6,7]

Multispecialty Articles · Original Research

Keywords

CT, effective dose, patient-specific organ dose, radiation burden characterization

Submitted: Oct 23, 2019
Revision requested: Dec 9, 2019
Revision received: Mar 9, 2020
Accepted: Apr 29, 2020

The authors declare that they have no disclosures relevant to the subject matter of this article.

Based on a presentation at the Radiological Society of North America 2018 annual meeting, Chicago, IL.

Supported in part by a grant from NIH (R01 EB001838). The technology has been nonexclusively licensed by Duke University to GE and Imalogix. Those entities were not involved in the development of the content of this article.

OBJECTIVE. The purpose of this study is to comprehensively implement a patient-informed organ dose monitoring framework for clinical CT and compare the effective dose (ED) according to the patient-informed organ dose with ED according to the dose-length product (DLP) in 1048 patients.

MATERIALS AND METHODS. Organ doses for a given examination are computed by matching the topogram to a computational phantom from a library of anthropomorphic phantoms and scaling the fixed tube current dose coefficients by the examination volume CT dose index ($CTDI_{vol}$) and the tube-current modulation using a previously validated convolution-based technique. In this study, the library was expanded to 58 adult, 56 pediatric, five pregnant, and 12 International Commission on Radiological Protection (ICRP) reference models, and the technique was extended to include multiple protocols, a bias correction, and uncertainty estimates. The method was implemented in a clinical monitoring system to estimate organ dose and organ dose–based ED for 647 abdomen-pelvis and 401 chest examinations, which were compared with DLP-based ED using a *t* test.

RESULTS. For the majority of the organs, the maximum errors in organ dose estimation were 18% and 8%, averaged across all protocols, without and with bias correction, respectively. For the patient examinations, DLP-based ED was significantly different from organ dose–based ED by as much as 190.9% and 234.7% for chest and abdomen-pelvis scans, respectively (mean, 9.0% and 24.3%). The differences were statistically significant ($p < .001$) and exhibited overestimation for larger-sized patients and underestimation for smaller-sized patients.

CONCLUSION. A patient-informed organ dose estimation framework was comprehensively implemented applicable to clinical imaging of adult, pediatric, and pregnant patients. Compared with organ dose–based ED, DLP-based ED may overestimate effective dose for larger-sized patients and underestimate it for smaller-sized patients.

Because of the widespread utility of CT in clinical diagnosis, its usage has increased steadily over the last decade. From recent estimates, about 82 million CT scans were performed in 2018 in the United States alone [1]. With the rise in the number of scans, it is beneficial to practice consistency and perform safety and quality control within and across institutions toward the general goal of increasing patient population safety by improving CT risk assessment and the design of effective optimization actions. Of particular interest is the estimation of radiation dose in clinical practice, which has prompted hospitals and clinics to record CT radiation dose from clinical examinations [2–4]. Most CT dose recordings are made according to system outputs and not patient dose. Yet radiation dose is an individualized burden to each patient, dependent on that patient's body attributes and the specific imaging protocol used. Individual patient dose is the attribute that necessitates the monitoring of radiation dose in the first place. Thus, radiation management would benefit from recording patient dose in an individualized, patient-specific manner accounting for age, size, and varying radiosensitivities of human tissues [5].

[1]Department of Radiology, Duke University, 2424 Erwin Rd, Ste 302, Durham, NC 27705. Address correspondence to W. Fu (wanyi.fu@duke.edu).

[2]Department of Electrical and Computer Engineering, Duke University, Durham, NC.

[3]Carl E. Ravin Advanced Imaging Laboratories, Duke University, Durham, NC.

[4]Clinical Imaging Physics Group, Duke University Health System, Durham, NC.

[5]Medical Physics Graduate Program, Duke University, Durham, NC.

[6]Department of Biomedical Engineering, Duke University, Durham, NC.

[7]Department of Physics, Duke University, Durham, NC.

doi.org/10.2214/AJR.19.22482

AJR 2021; 216:1–11

ISSN-L 0361–803X/21/2163–1

In making CT radiation dose records individualized, patient-specific organ dose and the corresponding organ dose–derived effective dose (ED_{OD}) have been regarded as the reference standard [6]. Estimating these quantities, however, requires explicit modeling of patient anatomy and CT scan geometry and protocols [7–9]. These tasks are both labor intensive and computationally expensive, which limits their feasibility and practicality in clinical implementation. As an alternative, scanner-derived exposure outputs, volume CT dose index ($CTDI_{vol}$), and dose-length product (DLP) that are recorded for each examination have been used to approximate effective dose according to DLP (ED_{DLP}) using DLP-to–effective dose (ED) conversion coefficients (*k* factors) [10–14]. However, the *k* factors are estimated with a sexless, ageless, uniform phantom and do not represent the varied attributes and organ distributions seen in patient populations. Consequently, these estimates may not represent the radiation burden to the patient with sufficient accuracy and precision.

To make the estimation of the radiation burden more specific to the patient, albeit not fully patient-specific, several studies have introduced patient-informed approaches, in which anticipated anatomic attributes of the patient are used to derive the patient organ dose estimates [15–18]. These methods are sometimes referred to as patient specific, even though the exact specifics of the patient are not modeled. As such, they are rather patient-informed because they rely on accessible patient attributes (e.g., patient diameter, sex) along with anthropomorphic models of the anatomy to inform the organ dose calculation. The computationally expensive modeling of the anatomy and radiation field is performed ahead of time and then ascribed to the patients, making the method practical for clinical applications. However, these methods have not yet been applied across the diversity of clinical protocols.

In this study, we aimed to develop and implement a comprehensive patient-informed organ dose estimation framework for clinical CT dose monitoring with enhanced accuracy, patient-cohort coverage, and protocol representation. To show its utility, patient-informed organ doses were calculated in two large CT clinical populations, and the results were used to determine the discrepancy between ED values derived from organ dose and DLP estimates.

Materials and Methods

This retrospective study was performed in compliance with HIPAA and was determined to be exempt from Duke University institutional review board requirements.

We describe the framework implementation and then its application to clinical CT images. The implementation includes creating necessary libraries and programs. Once implemented, the framework is applied to clinical CT images automatically. The workflow of the framework on clinical images is illustrated in Figure 1.

Framework Implementation

Modeling the anatomy—The study deployed an established patient-informed organ dose estimation method in which the anatomy for a given patient is modeled by matching it to a computational phantom from a library of anthropomorphic phantoms [19]. For this study, the library included extended cardiac-torso (XCAT) phantoms: 58 existing adult models, 56 existing pediatric models, 14 existing International Commission on Radiological Protection (ICRP) reference models, and five new pregnant models with 10 gestational ages of 3, 6, 8, 10, 15, 20, 25, 30, 35, and 38 weeks [9, 20–22]. The frontal views of phantom renderings are shown in Figure 2A. As described in separate publications for establishing the XCAT library, the adult and pediatric phantoms used in this study were created according to clinical CT images. Major organs were segmented using a semiautomatic process, and the remaining organs were added to the phantoms by deforming template models according to segmented organs from the National Library of Medicine Visible Human Project images [9, 20, 21, 23]. The ICRP reference phantoms used were made according to the template models, with the body and organ masses scaled according to ICRP 89 [22].

Specifically developed for this study, pregnant phantoms were formed according to five maternal models selected from existing adult female phantoms, representing different obesity classes (50th percentile height and weight; and body mass index [BMI], measured in weight in kilograms divided by the square of height in meters: underweight, 18.2; overweight, 28.6; class I obesity, 30.7; and class II obesity, 35.5). The fetus models were generated by segmenting organs and major structures from imaging data (CT, MRI, and histologic data). The maternal models were deformed to combine the fetus models and represent various gestational ages. The BMI and age of the XCAT models are shown in Figure 2B.

In the framework for organ dose estimation, the topogram of each patient was used to match to one phantom from the XCAT library according to anatomic landmark heights. Anatomic landmarks were automatically detected using a commercial software (DoseWatch, GE Healthcare) and included top and bottom of the head, shoulders, lungs, and pelvis. These landmarks determined patients' anatomic heights that were used as the criteria to find the closest matched phantom. This matching method thus approximated the patient anatomy to an anthropomorphic phantom with similar organ longitudinal distribution. The matching for pregnant patients was according to the longitudinal distribution and considering any of the modeled gestational ages.

When modeling exposure, the matched phantom was used to indicate patient's organ longitudinal distribution. The patient width was accommodated separately modeling with patient water equivalent diameter. The water equivalent diameter was automatically derived from the medium slice of the patient CT images (DoseWatch).

Modeling the exposure—The patient-informed organ doses were estimated accounting for the patient anatomy and the tube current modulation incorporating the $CTDI_{vol}$-to–organ dose conversion coefficients (*h* factors) [16, 18, 19, 24, 25]. The *h* factor library was created a priori for 13 adult protocols (chest, abdomen-pelvis, chest-abdomen-pelvis, abdomen, pelvis, liver, kidneys, kidney-to-bladder, adrenal, liver-to-kidneys, head, head-neck, neck) and six pediatric protocols (chest, abdomen-pelvis, chest-abdomen-pelvis, abdomen, pelvis, head) under constant tube current. For each XCAT phantom and protocol, the *h* factors were simulated by a previously validated Monte Carlo simulation package (PENELOPE, version 2006, Universitat de Barcelona) [7, 8, 26, 27]. For pregnant models, although a fetus at 3 and 6 weeks was created in our initial models, their volumes were too small to obtain credible dose values. Their doses were thus represented by the dose to the uterus. For a fetus older than 6 weeks, the fetus models included fetus bone structure and the rest as the fetus body and were considered as organs in the dose calculation. The *h* factors calcula-

TABLE 1: Summary of Simulated CT Techniques for Bias and Uncertainty Estimation

Cohort	Protocols	Tube Potential (kVp)	Bowtie Filter	Pitch	Collimation (mm)
Adult[a]					
Body	Chest, abdomen-pelvis, chest-abdomen-pelvis, abdomen, pelvis, liver, kidneys, kidney-to-bladder, adrenal, liver-to-kidneys	120	Large	1.375	40
Neuralgic	Head, head-neck, neck	120	Small	1	20
Pediatric					
Body	Chest, abdomen-pelvis, chest-abdomen-pelvis, abdomen, pelvis	120	Small	1.375	40
Neuralgic	Head	120	Small	1	20

Note—All CT techniques were conducted on a LightSpeed VCT (GE Healthcare) system.
[a]Adult cohort includes pregnant women.

tion used the normalized fetal-dose ratio method of Felmlee et al. [28]. The *h* factors were calculated for fetuses at various gestational ages and in maternal models with various sizes. Overall, within each protocol, the *h* factors were modeled as a function of the XCAT scanned region diameter applied to each new patient. For the pregnant phantoms, the *h* factors were applied to the patients according to both diameter and gestational ages.

The radiation field under modulated tube current was modeled as a function of the convolution of the tube current profile and a dose spread function using a previously developed technique [19]. The dose spread function was simulated by the Monte Carlo method on cylindric phantoms across diameters of 8–50 cm [19]. For each patient, the dose spread function corresponding to the patient diameter was used. The dose ratio was calculated as the ratio of dose spread function convolved with modulated tube current versus the dose spread function convolved with the mean tube current value with the same scan length [19]. The dose field for each organ ($CTDI_{organ}$) was determined according to the dose ratio with respect to organ distribution from the matched XCAT phantom and the examination $CTDI_{vol}$ [19]. The examination $CTDI_{vol}$ accommodates radiation specification from various scanners and CT techniques. The organ dose was calculated as a function of the $CTDI_{organ}$ and *h* factor [19].

Bias and uncertainties—Organ doses estimated by the proposed method showed bias and uncertainties compared with those simulated using the Monte Carlo method (the reference standard) [19]. To improve the accuracy of the estimated organ doses, we developed a secondary correction and uncertainty estimation strategy using simulated CT scans with known organ dose ground truth. Simulated CT scans were conducted for each XCAT phantom and protocol using typical clinical CT examination protocols. The CT techniques are shown in Table 1. All examinations simulated tube current modulation according to Li et al. [29]. The organ dose estimated using the proposed method (OD_C) was obtained in a leave-one-out method in which each XCAT phantom was treated as a new patient, matched to another XCAT to obtain the OD_C from the exposure model as proposed. The ground truth organ dose (OD_M) was estimated using a validated Monte Carlo simulation package [17]. The statistics of OD_C and OD_M were used to generate linear models that provided organ doses with bias correction (OD_{CB}) and CIs on new clinical patients within each cohort, protocol, and organ. Specifically, a linear fit was applied to OD_C versus OD_M for each protocol, cohort (each gestational age for pregnant phantoms), and organ as

$$OD_M = \beta_0 OD_C + \beta_1 + \varepsilon, \quad (1)$$

where β_0 and β_1 are fitting coefficients and ε is the fitting error. The fits were used to provide bias-corrected, protocol-specific organ dose values ($OD_{CB,p}$, where *p* denotes a patient) and 95% CI as

$$OD_{CB,p} = \widehat{\beta_0} OD_{C,p} + \widehat{\beta_1} \quad (2)$$

and

$$CI = t_{\frac{\alpha}{2},N} RMSE \sqrt{1 + \frac{1}{N} + \frac{(OD_{C,p} - \overline{OD_C})^2}{\sigma^2_{OD_C}}} \quad (3)$$

where β_0 hat and β_1 hat are the estimated coefficients obtained from fitting model (Equation 1) to the data. $OD_{C,p}$ is the organ dose estimated for a new patient, *N* is the number of phantoms, the expression of *t* is the *t* value with $N - 2$ degrees of freedom, *RMSE* is the root mean square error between OD_C and OD_M for all phantoms of the protocol and cohort, and OD_C with the overbar and corresponding σ^2 are the mean and variance of OD_C, respectively.

Framework accuracy—To quantify the overall organ dose estimation accuracy within this XCAT library, the mean difference between the estimated dose using the leave-one-out method (either OD_C or OD_{CB}) and OD_M was calculated for each protocol.

Clinical Study

Patients and scan protocols—The framework was tested across 1048 patients (mean age, 58 years; range, 18–89 years) who underwent abdomen-pelvis scans with contrast enhancement (647 examinations) or chest scans without contrast enhancement (401 examinations) from January 5, 2017, to August 29, 2018, at Duke University. Cases included 524 women (mean age, 57 years; range, 18–88 years) and 524 men (mean age, 59 years; range, 18–89 years). All image data were acquired using a commercial scanner (Discovery CT750 HD, GE Healthcare) with tube current modulation, a tube voltage of 120 kV, and pitch values of 1.53 for chest and 0.98 or 1.53 for abdomen-pelvis scans.

Effective dose estimation and data analysis—For each examination, the ED was calculated using two methods evaluated in this study according to the patient-informed organ dose estimated using the proposed method as

$$ED_{OD,p} = \sum_o OD_{BC,p} w_o, \quad (4)$$

where p denotes a patient and w_o is the tissue weighting coefficients defined by ICRP Publication 103 [30]; and according to DLP as

$$ED_{DLP,p} = \sum_r DLP_{r,p} k_{r,p}, \quad (5)$$

where $DLP_{r,p}$ is the DLP for region r (e.g., chest, abdomen-pelvis); and k_r is the DLP-to-ED conversion coefficients for region r defined by ICRP Publication 102 [6]. The mean difference between $ED_{OD,p}$ and $ED_{DLP,p}$ was calculated for each protocol and evaluated using a t test (Matlab, version 2018a, Mathworks) in terms of the difference across all patients and across different-sized groups (grouped according to the water equivalent diameter). Although some other investigators have used the ICRP reference phantom for the purpose of overall radiation exposure estimation [30], this study calculated the $ED_{OD,p}$ for each patient using a virtual anthropomorphic phantom matched to the patient.

Results

Extended Cardiac-Torso Phantom Validation

Figure 3 shows OD_M versus OD_C and OD_{CB} and their corresponding linear model for sample protocols. The OD_C was correlated with OD_M for organs inside, on the periphery, outside, and distributed (R, 0.78 ± 0.24 [SD]; 0.62 ± 0.28; 0.34 ± 0.33; 0.63 ± 0.31, respectively), and averaged across all protocols, cohorts, and organs within each location group according to Sahbaee et al. [17]. The linear model with bias correction obtained unified the slope and reduced the intercept.

Figure 4 shows the difference between OD_M versus OD_C and OD_{CB} for each organ and protocol averaged across all of the XCAT phantoms within each cohort. When accounting for all the organs, the protocol-averaged maximum error was 53% and 18%, without and with bias correction, respectively. The corresponding errors within each cohort were 53% (adult), 56% (pregnant), and 45% (pediatric) without bias correction, and 21% (adult), 13% (pregnant), and 17% (pediatric) with bias correction. When accounting for the majority of organs (excluding 15% of outlier organs with the largest errors), the protocol-averaged maximum errors were 18% and 8%, without and with bias correction, respectively. The corresponding errors within each cohort were 17% (adult), 18% (pregnant), and 17% (pediatric) without bias correction, and 9% (adult), 7% (pregnant), and 8% (pediatric) with bias correction. As shown, for the majority of organs, including fetus as an organ, the dose estimation showed reasonable errors, and the error reduced with bias correction. The bias correction was more effective for organs with larger errors.

Clinical Study

Figure 5 shows the liver, lung, and bone-surface organ doses as a function of examination mean $CTDI_{vol}$ for the 401 chest and 647 abdomen-pelvis scans. The plots indicate that for each examination mean $CTDI_{vol}$, different organs have diverse dose values. For chest scans, the lung-to-liver and lung-to-bone dose differences were 36.7% ± 9.6% and 52.7% ± 5.4% of the $CTDI_{vol}$, respectively, averaged across all chest examinations. For abdomen-pelvis scans, the liver-to-lung and liver-to-bone dose differences were 67.0% ± 22.5% and 26.8% ± 12.3% of $CTDI_{vol}$, respectively, averaged across all abdomen-pelvis examinations.

Figure 6 shows the ED as a function of water equivalent diameter for the 401 chest and 647 abdomen-pelvis scans. ED_{DLP} was, on average, greater than ED_{OD} by 9.0% ($p < .001$, range from –18.1% to 190.9%) and 24.3% ($p < .001$, range from –28.4% to 234.7%) for chest and abdomen-pelvis scans, respectively. For water equivalent diameter ranges of less than 25, 25–30, 30–35, and greater than 35 cm, the percentage differences between ED_{DLP} and ED_{OD} were –6.3% ± 21.8% ($p < .001$), 8.8% ± 21.2% ($p < .001$), 31.6% ± 34.9% ($p < .001$), and 38.3% ± 11.0% ($p = .04$) for chest, and –13.3% ± 14.3% ($p < .001$), 4.4% ± 18.1% ($p < .001$), 31.3% ± 25.1% ($p < .001$), and 61.9% ± 32.2% ($p < .001$) for abdomen-pelvis protocols. On group average, ED_{DLP} was larger than ED_{OD} for larger patients (water equivalent diameter, > 25 cm) and smaller than ED_{OD} for smaller patients (water equivalent diameter, < 25 cm).

Discussion

In the wake of accreditation and regulatory program requirements, an increasing number of hospitals and clinics are recording radiation dose from CT examinations. When combined with image quality or other diagnostic performance measurements, they can be used to manage exposure and optimize imaging protocols. To facilitate this management, it is best to use metrics that are most relevant to the actual burden on a patient. Current clinical practice typically relies on scanner-derived dose indexes such as $CTDI_{vol}$ and DLP, which are more of a reflection of the exposure output of the machine than the actual radiation burden to the patient. Patient-specific approaches require time-consuming and labor-intensive anatomic modeling of each patient and computationally expensive Monte Carlo simulations, which although accurate, are challenging in clinical applications. In this study, we implemented a comprehensive patient-informed organ dose estimation framework. The patient information is taken into account and precalculated anatomy and exposure datasets are used to provide clinical dose estimation in real time and with high accuracy. This system may assist in exposure standardization and comparison within and across health care providers and potentially protocol optimization when combined with diagnostic image quality–related measurements.

To facilitate exposure management, ED according to organ doses and tissue weighting coefficients is a relevant quantity, accounting for the actual radiation burden to the patient. Organ doses determined in a patient-relevant manner, however, are usually not known. In such cases, ED according to DLP is commonly used. The difference between the two quantities has previously been noted for a limited number of protocols and reference phantoms under fixed tube current condition [12–14]. In this study, the comparison was performed under a widely used modulated tube current condition in a clinical population. The ED from patient-informed organ dose showed a substantial difference from those estimated using the DLP method. This difference can be as large as –28.4% to 234.7%, with the differences larger for larger-sized patients. This suggests that care should be exercised when using

ED_{DLP} to inform clinical decisions, because overestimating doses may lead to unnecessary concern and result in insufficient exposures, and vice versa.

There is an increase in the ED with increased patient size, which agrees with previous studies reporting the ED according to patient-specific organ doses [15, 31]. Our clinical study showed that ED_{DLP} is overestimated for larger patients and underestimated for smaller patients. This trend agrees with a clinical study on abdomen-pelvis examinations with tube current modulation by Haji-Momenian et al. [14], who explained that this trend was a result of using size-generic *k* factors [31]. In a previous work deriving patient-specific *k* factors using patient-specific organ dose, the patient-specific *k* factors were shown to decrease with increased patient size [15, 31]. Moreover, Haji-Momenian et al. [14] reported that ED_{DLP} agreed with ED_{OD} for patients with a diameter of 28 cm, matching the diameter of phantoms used to derive the generic *k* factors commonly used for ED_{DLP} calculation [32]. Our study confirmed that there is a better agreement between ED_{DLP} and ED_{OD} for patients with water equivalent diameter ranging from 25 to 30 cm, with ED_{DLP} being underestimated for patients smaller than 25 cm and overestimated for patients larger than 30 cm. This is likely a result of the fact that in larger-sized patients, remainder tissue consists of more volume, and this radiation sensitivity distribution change is not taken into account in ED_{DLP}. As shown, the DLP-based method may likely overestimate the dose for larger-sized patients and underestimate for the smaller patients. The underestimation for dose can negatively affect risk assessment (for pediatric patients), whereas overestimation can compromise needed quality for image protocols. Therefore, only a robust and consistent dose estimate for both cohorts can ensure the evaluation and the design of optimal radiologic procedures.

There are a few limitations in this study. First, the organ dose estimation system accuracy was only validated for one scanner. Different hospitals may use different scan protocols. Although it was not performed in the current study, the same method can be extended to other scanners and manufacturers. The differences in dose among scanners and CT techniques have been shown to be largely normalized by using the $CTDI_{vol}$; thus, when implementing the framework we used quantities normalized by the $CTDI_{vol}$ [16, 25]. In the application, the examination $CTDI_{vol}$ is used as a parameter to address the radiation field under different scanners and CT techniques with tube current modulation separately incorporated in the calculation. Second, the XCAT dataset was used both to create and validate the system. This was done because it is time and resource expensive to create accurate computational phantoms. In future work we will examine a completely different dataset to validate the overall system. Furthermore, the framework implementation is portable to other phantom libraries. The users may use alternative libraries either publicly available or through licensing. Third, in the clinical study the ED did not have a corresponding ground truth to address the accuracy of ED_{OD} and ED_{DLP}. However, compared with ED_{DLP}, ED_{OD} considers heterogeneity in both the tissue radiation sensitivity and tube current modulation radiation field, which in theory is more accurate and relevant to the patient dose. Fourth, the study focused on organ dose–based ED estimation on clinical images and did not investigate other alternative patient-informed metrics such as size-specific dose estimate and the dose estimation using size-specific conversion factors [33–35]. However, future studies can extend our approach to include the comparison with other patient-informed radiation metrics. Finally, the clinical study was limited to the adult population without any confirmed cases of pregnancy. Future work will include pediatric populations.

In conclusion, in this study we comprehensively implemented and showed the feasibility of a patient-informed organ dose monitoring system in the clinical setting. Compared with scanner-derived dose indexes such as $CTDI_{vol}$ or DLP, the system provides a more accurate estimate of organ dose by taking into account variation of tissue radiation sensitivity and heterogeneity in the radiation field, especially under tube current modulation. Of notable innovation, the framework provides for estimation of fetal dose under variable habitus and gestational conditions.

References

1. IMV Medical Information Division. *2018 CT Market Outlook Report*. IMV, 2018
2. McCollough CH, Chen GH, Kalender W, et al. Achieving routine submillisievert CT scanning: report from the summit on management of radiation dose in CT. *Radiology* 2012; 264:567–580
3. Brenner DJ, Hall EJ. Computed tomography: an increasing source of radiation exposure. *N Engl J Med* 2007; 357:2277–2284
4. Schauer DA, Linton OW. NCRP Report No. 160, ionizing radiation exposure of the population of the United States, medical exposure: are we doing less with more, and is there a role for health physicists? *Health Phys* 2009; 97:1–5
5. Jaffe TA, Yoshizumi TT, Toncheva G, et al. Radiation dose for body CT protocols: variability of scanners at one institution. *AJR* 2009; 193:1141–1147
6. Valentin J; International Commission on Radiological Protection. Managing patient dose in multi-detector computed tomography (MDCT): ICRP publication 102. *Ann ICRP* 2007; 37:1–79, iii
7. Li X, Samei E, Segars WP, et al. Patient-specific radiation dose and cancer risk estimation in CT. Part I. Development and validation of a Monte Carlo program. *Med Phys* 2011; 38:397–407
8. Li X, Samei E, Segars WP, et al. Patient-specific radiation dose and cancer risk estimation in CT. Part II. Application to patients. *Med Phys* 2011; 38:408–419
9. Segars WP, Bond J, Frush J, et al. Population of anatomically variable 4D XCAT adult phantoms for imaging research and optimization. *Med Phys* 2013; 40:043701
10. Christner JA, Kofler JM, McCollough CH. Estimating effective dose for CT using dose-length product compared with using organ doses: consequences of adopting International Commission on Radiological Protection publication 103 or dual-energy scanning. *AJR* 2010; 194:881–889
11. McCollough CH, Christner JA, Kofler JM. How effective is effective dose as a predictor of radiation risk? *AJR* 2010; 194:890–896
12. Newman B, Ganguly A, Kim JE, Robinson T. Comparison of different methods of calculating CT radiation effective dose in children. *AJR* 2012; 199:[web]W232–W239
13. Brady SL, Mirro AE, Moore BM, Kaufman RA. How to appropriately calculate effective dose for CT using either size-specific dose estimates or dose-length product. *AJR* 2015; 204:953–958
14. Haji-Momenian S, Ellenbogen A, Khati N, et al. Comparing dose-length product-based and Monte Carlo simulation organ-based calculations of effective dose in 16- and 64-MDCT examinations using automatic tube current modulation. *AJR* 2018; 210:583–592
15. Ding A, Mille MM, Liu T, Caracappa PF, Xu XG. Extension of RPI-adult male and female computational phantoms to obese patients and a Monte Carlo study of the effect on CT imaging dose. *Phys Med Biol* 2012; 57:2441–2459
16. Turner AC, Zhang D, Khatonabadi M, et al. The feasibility of patient size-cor-

rected, scanner-independent organ dose estimates for abdominal CT exams. *Med Phys* 2011; 38:820–829
17. Sahbaee P, Segars WP, Samei E. Patient-based estimation of organ dose for a population of 58 adult patients across 13 protocol categories. *Med Phys* 2014; 41:072104
18. Tian X, Li X, Segars WP, Paulson EK, Frush DP, Samei E. Pediatric chest and abdominopelvic CT: organ dose estimation based on 42 patient models. *Radiology* 2014; 270:535–547
19. Tian X, Segars WP, Dixon RL, Samei E. Convolution-based estimation of organ dose in tube current modulated CT. *Phys Med Biol* 2016; 61:3935–3954
20. Segars WP, Sturgeon G, Mendonca S, Grimes J, Tsui BM. 4D XCAT phantom for multimodality imaging research. *Med Phys* 2010; 37:4902–4915
21. Segars WP, Norris H, Sturgeon GM, et al. The development of a population of 4D pediatric XCAT phantoms for imaging research and optimization. *Med Phys* 2015; 42:4719–4726
22. Stabin M, Emmons MA, Segars WP, Fernald M, Brill AB. ICRP 89-based adult and pediatric phantom series. *J Nucl Med* 2008; 49(suppl 1):14P
23. National Library of Medicine website. Download Visible Human Project data. www.nlm.nih.gov/databases/download/vhp.html. Accessed January 8, 2020
24. Ding A, Gao Y, Liu H, et al. VirtualDose: a software for reporting organ doses from CT for adult and pediatric patients. *Phys Med Biol* 2015; 60:5601–5625
25. Turner AC, Zankl M, DeMarco JJ, et al. The feasibility of a scanner-independent technique to estimate organ dose from MDCT scans: using CTDIvol to account for differences between scanners. *Med Phys* 2010; 37:1816–1825
26. Badal A, Badano A. Accelerating Monte Carlo simulations of photon transport in a voxelized geometry using a massively parallel graphics processing unit. *Med Phys* 2009; 36:4878–4880
27. Baro J, Sempau J, Fernández-Varea J, Salvat F. PENELOPE: an algorithm for Monte Carlo simulation of the penetration and energy loss of electrons and positrons in matter. *Nucl Instrum Methods Phys Res B* 1995; 100:31–46
28. Felmlee JP, Gray J, Leetzow M, Price J. Estimated fetal radiation dose from multislice CT studies. *AJR* 1990; 154:185–190
29. Li X, Segars WP, Samei E. The impact on CT dose of the variability in tube current modulation technology: a theoretical investigation. *Phys Med Biol* 2014; 59:4525–4548
30. Valentin J, ed. *The 2007 recommendations of the International Commission on Radiological Protection, ICRP publication 103*. Elsevier, 2007
31. Li X, Samei E, Williams CH, et al. Effects of protocol and obesity on dose conversion factors in adult body CT. *Med Phys* 2012; 39:6550–6571
32. Cristy M, Eckerman K. Specific absorbed fractions of energy at various ages from internal photon sources. Oak Ridge National Laboratory, 1987: ORNL/TM-8381
33. Boone JM. Reply to "comment on the 'report of AAPM TG 204: size-specific dose estimates (SSDE) in pediatric and adult body CT examinations'" [AAPM Report 204, 2011]. (letter) *Med Phys* 2012; 39:4615–4616
34. McCollough C, Bakalyar DM, Bostani M, et al. Use of water equivalent diameter for calculating patient size and size-specific dose estimates (SSDE) in CT: the report of AAPM task group 220. *AAPM Rep* 2014; 2014:6–23
35. Romanyukha A, Folio L, Lamart S, Simon SL, Lee C. Body size-specific effective dose conversion coefficients for CT scans. *Radiat Prot Dosimetry* 2016; 172:428–437

(Figures start on next page)

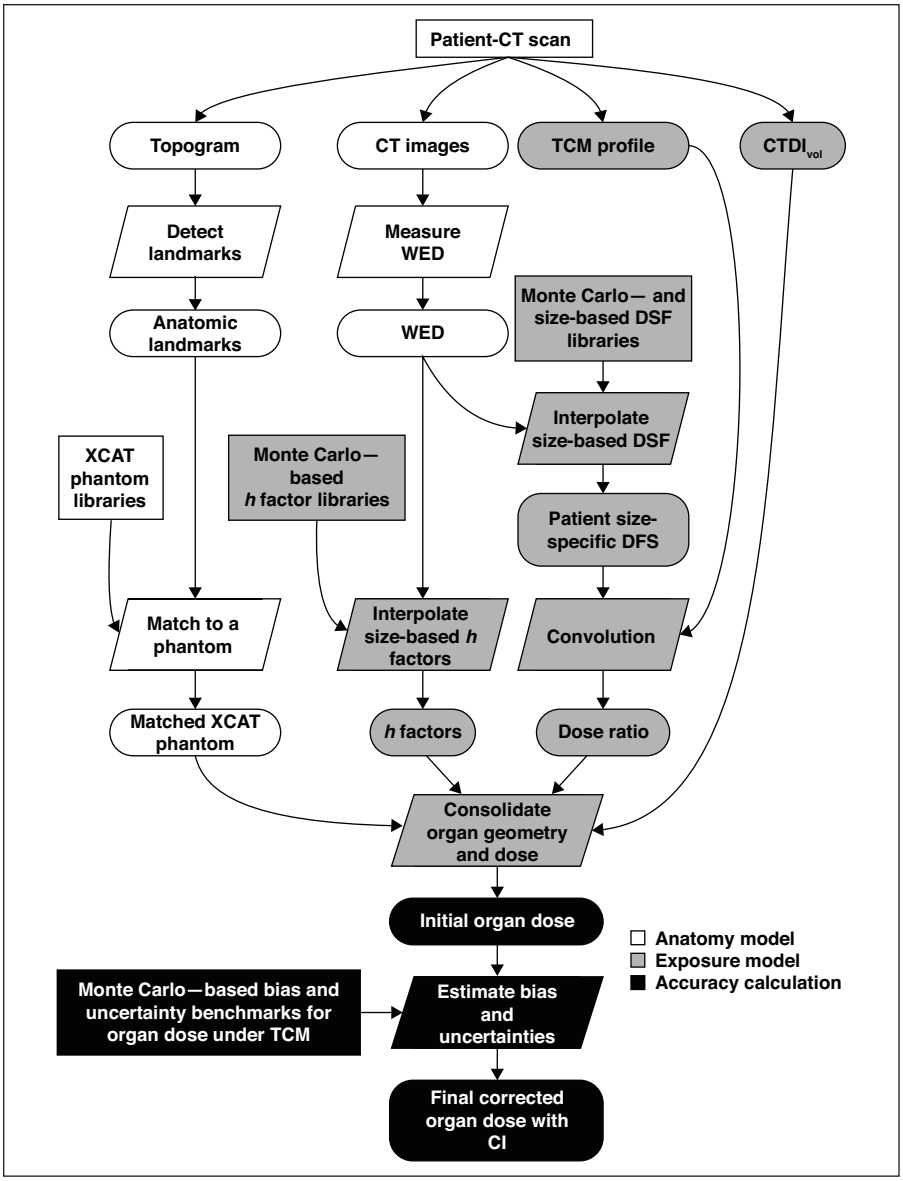

Fig. 1—Flowchart shows clinical organ dose estimation framework used in this study. Rectangles indicate precomputed data; ovals represent data generated during computation; parallelograms represent calculation. *h* factors are CT dose index–to–organ dose conversion coefficients. TCM = tube current modulation, $CTDI_{vol}$ = volume CT dose index, WED = water equivalent diameter, DSF = dose spread function, XCAT = extended cardiac-torso phantom.

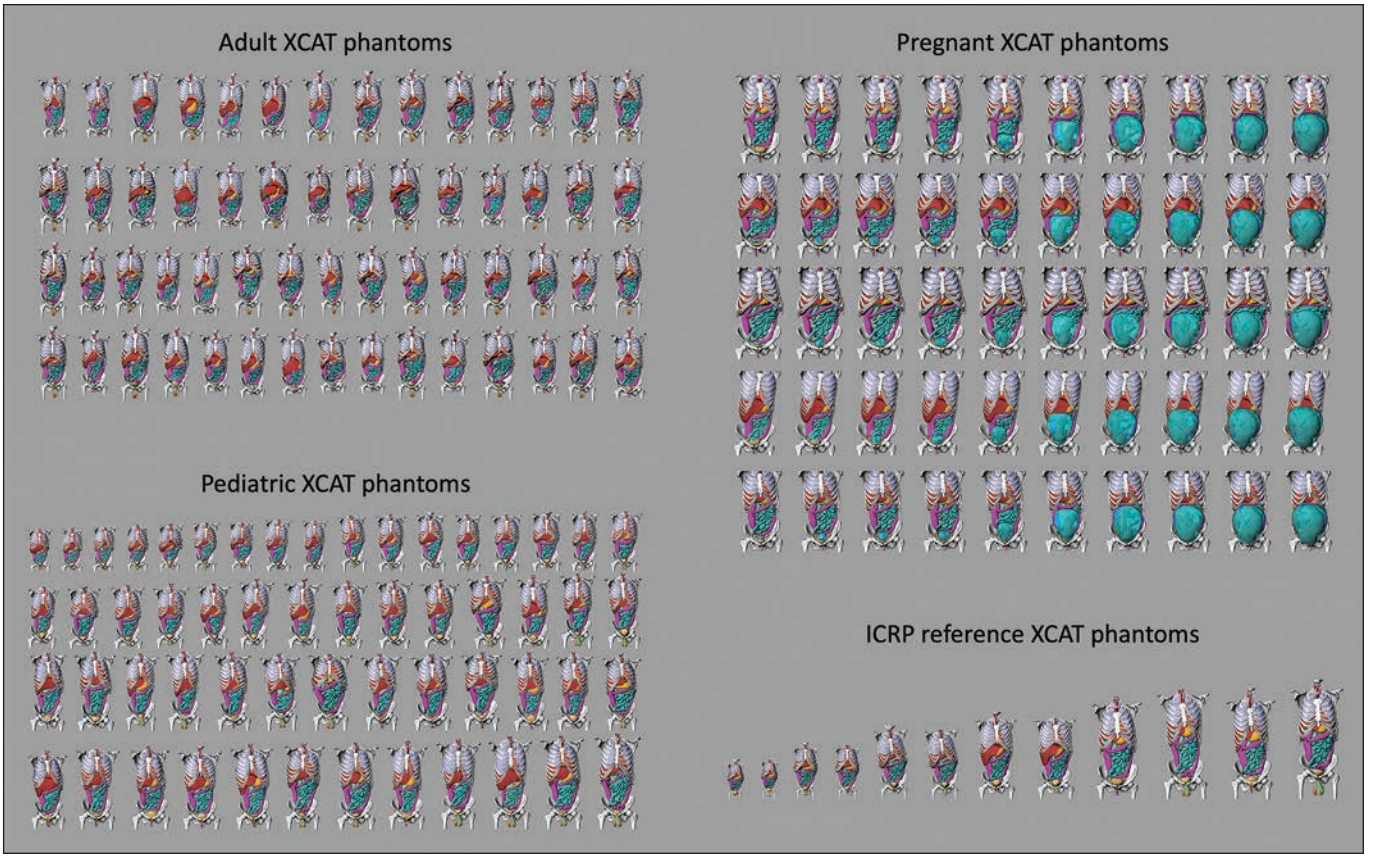

A

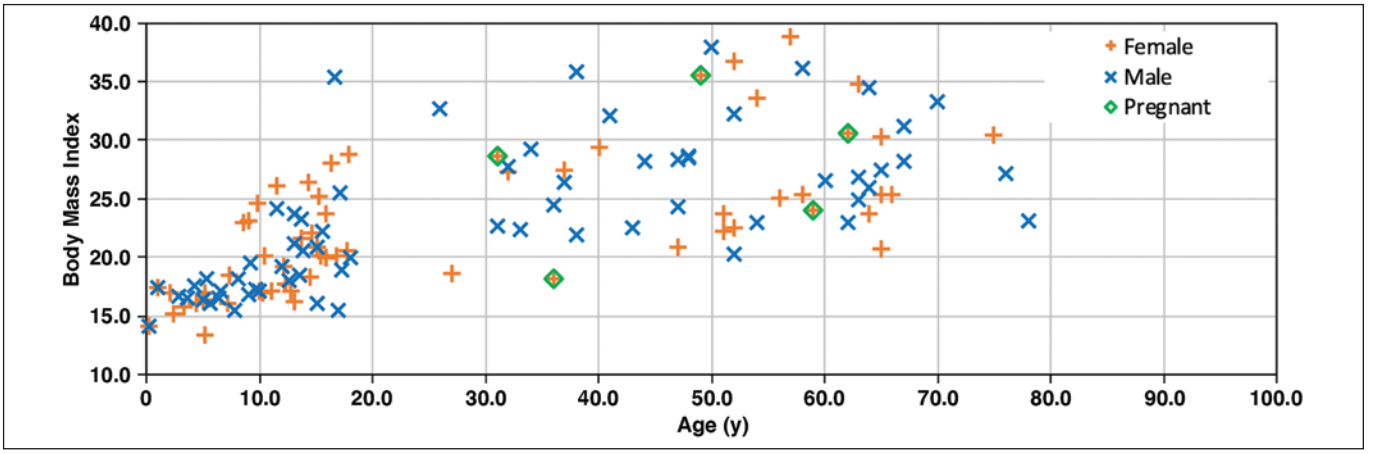

B

Fig. 2—Extended cardiac-torso (XCAT) phantoms used in study.
A, Chart shows frontal views of phantoms of 58 adults (age range, 18–78 years; 23 women, 35 men), 56 pediatric patients (age range, 2–18 years; 31 girls, 25 boys), five pregnant women (gestational age range, 3–38 weeks), and 12 International Commission on Radiological Protection (ICRP) reference XCAT phantoms used in this study. Phantom skin, head, arm, and legs were removed to enhance visualization of organs in chest-abdomen-pelvis region.
B, Graph shows body mass index and age of XCAT phantom variations within population.

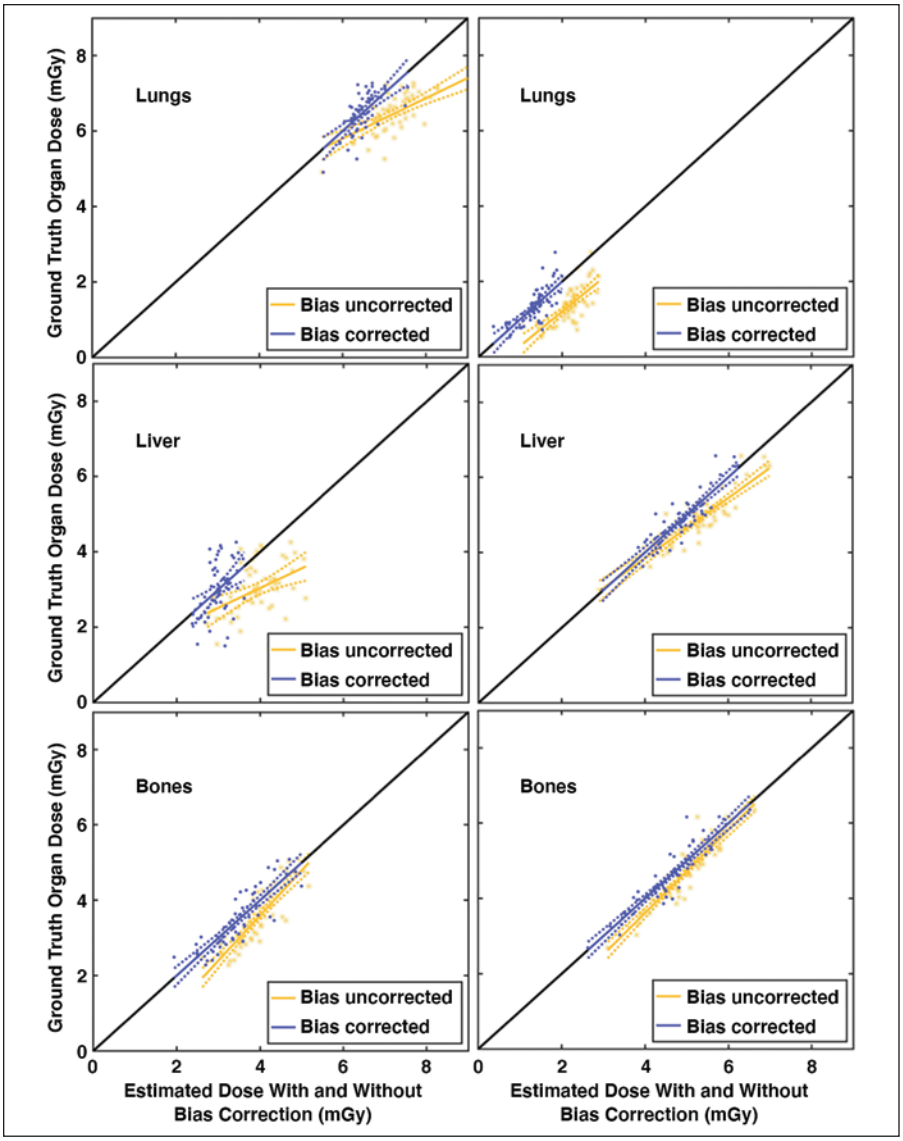

Fig. 3—Linear models of ground truth (Monte Carlo simulation) organ dose (OD_M) plotted against estimated dose (present study) without (OD_C) and with (OD_{CD}) bias correction for adult chest (*left*) and abdomen-pelvis (*right*) protocols. Each dot represents dose obtained from one phantom. Identity line is plotted in black; ideally all points lie on this diagonal line. Dashed lines represent CIs of linear model. Lungs (*top*), liver (*middle*), and bone surface (*bottom*) were chosen to represent organ on peripheral (inside), inside (on peripheral), or distributed for chest (abdomen-pelvis) protocols with respect to scan coverage.

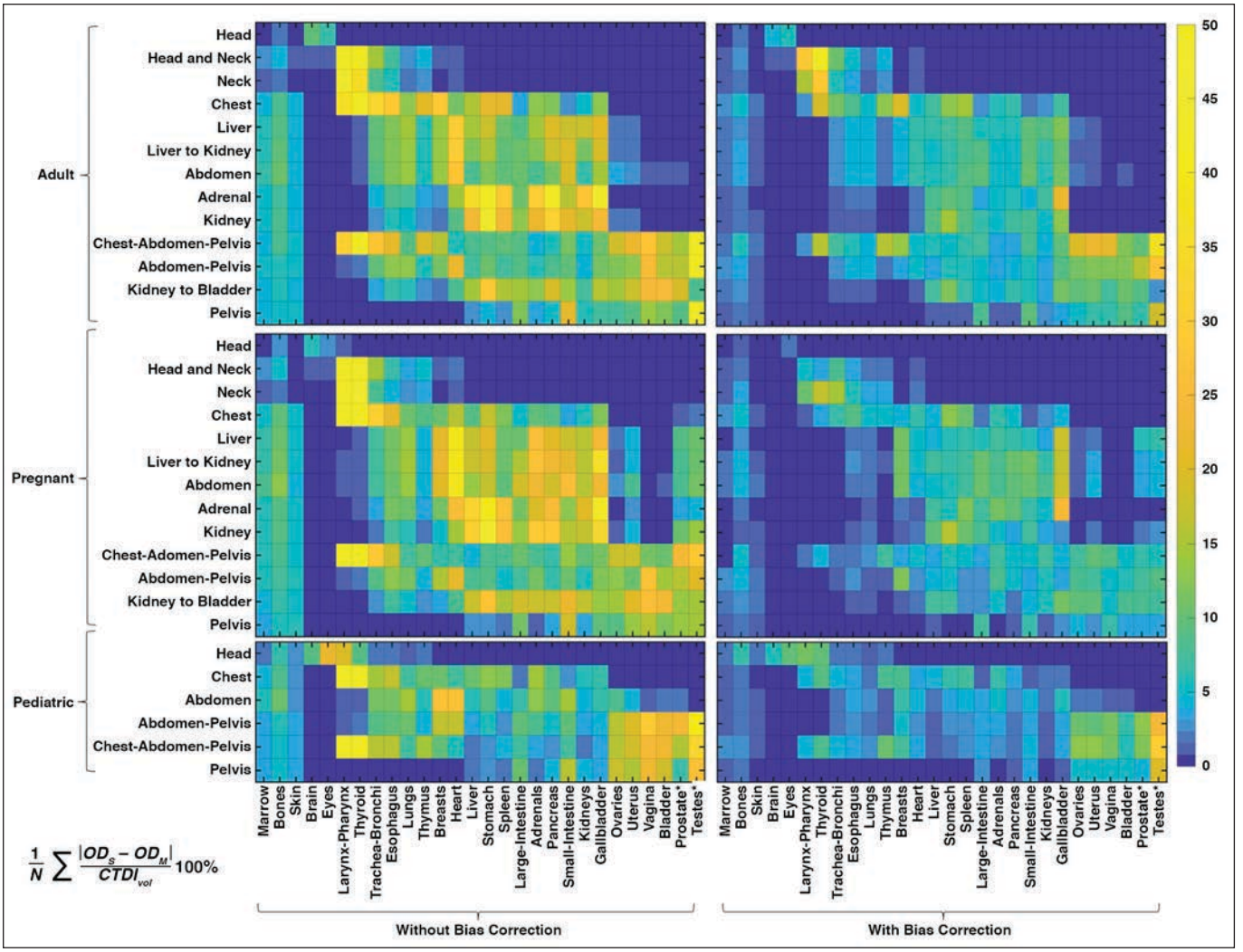

Fig. 4—Maps of errors of organ dose estimation with and without bias correction, compared with ground truth (Monte Carlo) simulation averaged among phantoms in adult, pregnant, and pediatric cohorts for each organ protocol. Error was calculated as indicated in equation at bottom of figure, where *N* is number of phantoms, and OD_S and OD_M are organ dose estimated in this study and by Monte Carlo simulation, respectively. Asterisk represents fetus body and fetus bone tissue for pregnant cohort. Gradient scale indicates errors of organ dose estimation (%).

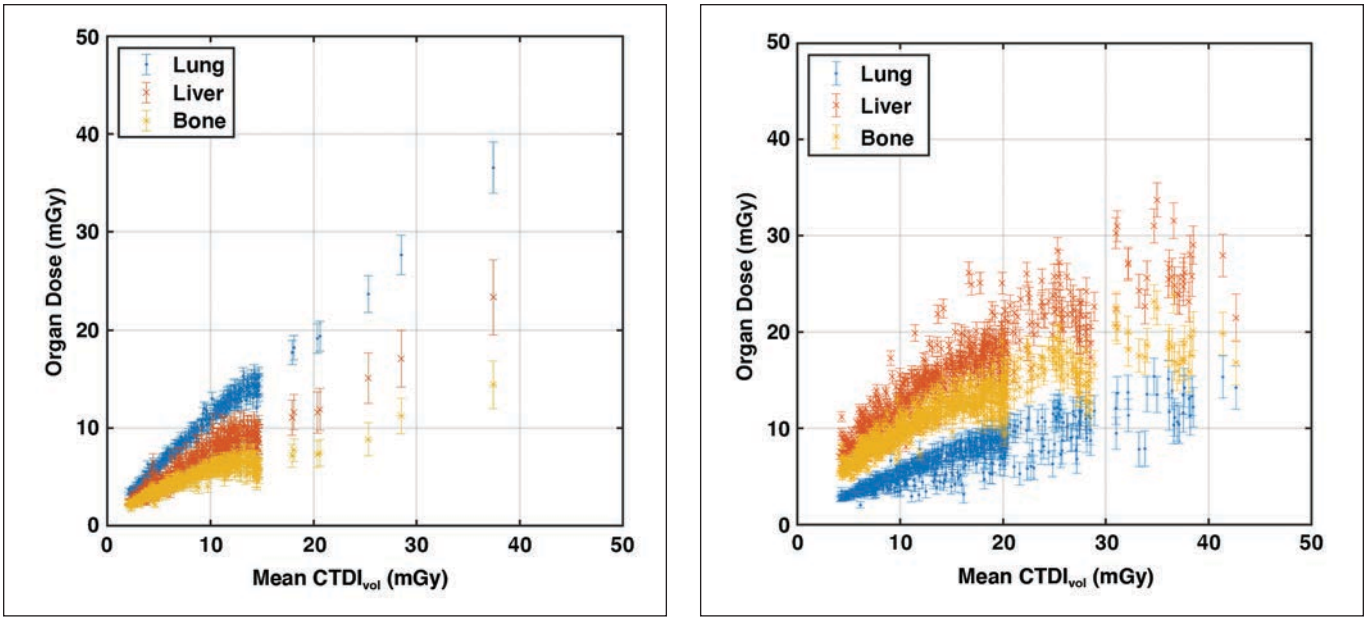

Fig. 5—Organ doses plotted against volume CT dose index ($CTDI_{vol}$). Error bars represent 95% CI.
A, Graph shows 401 chest examinations (mean age, 61 years; range, 18–88 years) including 170 women and 231 men.
B, Graph shows 647 abdomen–pelvis examinations (mean age, 56 years; range, 18–89 years) including 354 women and 293 men.

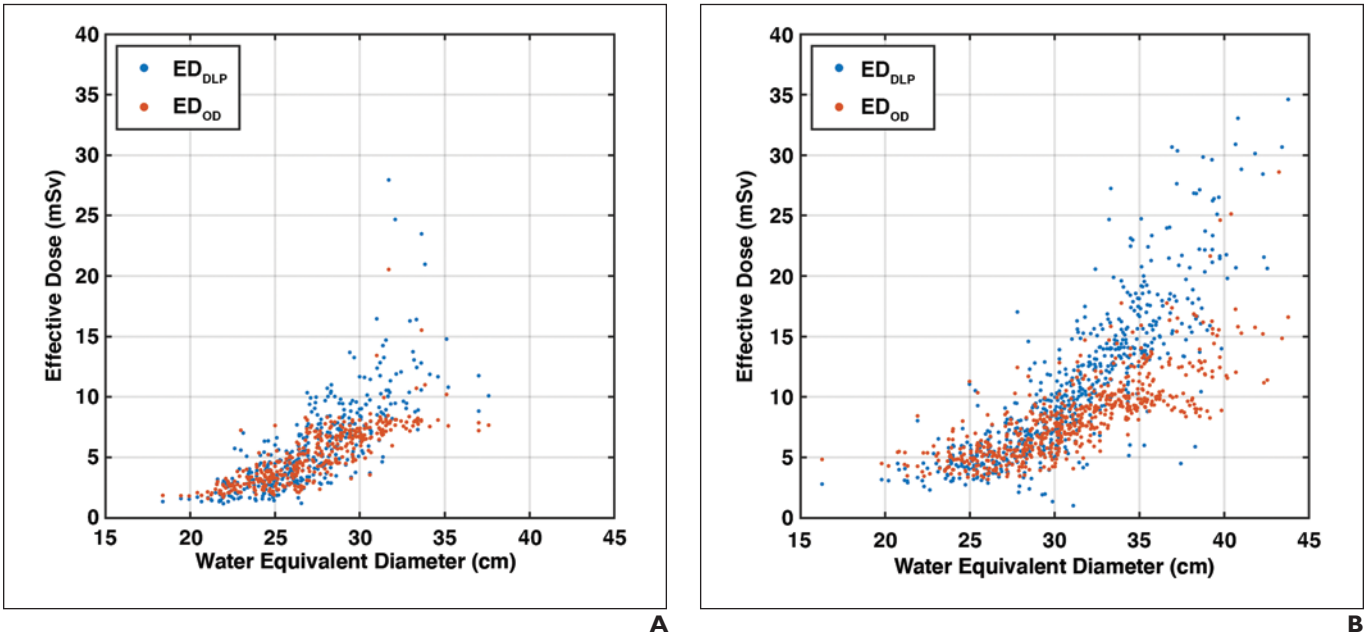

Fig. 6—Organ dose–based effective dose (ED_{OD}) and dose-length-product–based effective dose (ED_{DLP}) plotted against water equivalent diameter. ED_{DLP} shows higher values compared with ED_{OD} for larger-sized patients and lower values for smaller-sized patients.
A, Graph shows data for 401 chest examinations (mean age, 61 years; range, 18–88 years) including 170 women and 231 men.
B, Graph shows data for 647 abdomen-pelvis examinations (mean age, 56 years; range, 18–89 years) including 354 women and 293 men.